Experimental Thermal and Fluid Science 97 (2018) 364–374

Contents lists available at ScienceDirect

Experimental Thermal and Fluid Science

journal homepage: www.elsevier.com/locate/etfs

Pendant drops shed from a liquid lens formed by liquid draining down the inner wall of a wide vertical tube

M.W.L. Chee, S. Balaji, G.L. Cuckston, J.R. Davidson, D.I. Wilson*

Department of Chemical Engineering and Biotechnology, Philippa Fawcett Drive, West Cambridge Site, Cambridge CB3 0AS, UK

ARTICLE INFO

Keywords:
Pendant drop
Draining film
Surface tension
Instability

ABSTRACT

When a viscous liquid empties from an initially full, wide vertical tube, the drainage behaviour changes from a filament to a regime in which individual drops are shed by a lens formed at the end of the tube: liquid drains down the wall and the lens grows until it becomes unstable. This drop shedding regime was investigated for four Newtonian liquids (rapeseed oil, glycerol, honey and golden syrup) in three tube sizes and two tube materials (Bond number based on tube i.d. > 1 in all cases). The drop mass increased modestly with flow rate and the equivalent sphere diameter, d, was strongly related to the capillary length $L_c \equiv (\gamma/\rho g)^{1/2}$ rather than the tube diameter. The results were fitted to a correlation of the form $d/L_c = f$(Bond, Reynolds, Morton, sine of the contact angle) derived from dimensional analysis. The data were compared with existing models for drop formation from filled narrow capillaries and a new, simple model based on a quasi-static model of the lens. Agreement with these models was poor, particularly for larger tubes, indicating the need for more detailed analysis. Insights into the dynamics, generated by video analysis of the lens shape, are presented.

1. Introduction

The formation of drops by a liquid as it drains out of a vertical tube has been studied for some time [11] and is widely used for the determination of surface tension, either by measuring the weight of successive drops [7] (see review [8]); or by analysing the shape of a pendant drop (reviewed by Berry et al. [4]). The evolution of the shape of the liquid as it approaches pinch-off to create a drop and the relationship between the drop volume and the tube diameter was first considered for Newtonian fluids by Rayleigh: the Rayleigh instability has since been considered for other types of fluid (*e.g.* Balmforth et al. [2], Balmforth et al. [3]).

Drop weight tests employ relatively narrow tubes or capillaries. Periodic drop formation is also observed when a viscous liquid drains from a wide upright tube which is open to the atmosphere at both ends. This behaviour was reported by Ali et al. [1] in their experimental study of the self-drainage of viscous food-related liquids in process pipework: their aim was to establish how much liquid (*i.e.* product) could thereby be removed from a tube before introducing a flow of cleaning agent to flush it out. As the liquid drains from the base of the tube as a long filament, air enters from the top of the tube in the form of a long slug (see Fig. 1(a)). When the slug nose approaches the base of the tube, it does not break through but halts and the filament breaks, creating a liquid lens (Fig. 1(b)) [See Supplementary Videos A and B]. As liquid is steadily added to the lens from the draining annular film, the lens increases in size (Fig. 1(c)) until it becomes unstable, shedding a drop and reforming the lens (Fig. 1(d)). The cycle repeats itself.

* Corresponding author.
E-mail address: diw11@cam.ac.uk (D.I. Wilson).

https://doi.org/10.1016/j.expthermflusci.2018.04.015
Received 13 February 2018; Received in revised form 28 March 2018; Accepted 17 April 2018
Available online 19 April 2018

Nomenclature

Roman

a_1	constant, Eqs. (27) and (28)
a_2	constant, Eqs. (27) and (28)
a_3	constant, Eq. (27)
Bo	Bond number
d	drop equivalent sphere diameter
D	tube inner diameter
f	Eq. (2)
f_1	Eq. (3)
f_2	Eq. (4)
F	filament diameter
Fr	Froude number
Fr_c	Froude number (characteristic velocity is associated with flow in a capillary)
g	acceleration due to gravity
Ga	Galilei number
h	minimum meniscus thickness
L_c	capillary length
m	drop mass
m_{lens}	lens mass at critical point
m_{total}	total mass on scale
M	mass flow rate in draining annular film
M_c	mass flow rate in draining annular film of thickness L_c
M^*	dimensionless mass flow rate, $M^* = M/M_c$
Mo	Morton number
P_{atm}	atmospheric pressure
P_b	liquid pressure at the tube outlet ($z = 0$)
$P_{L,int}$	local hydrostatic pressure on the liquid side of the lens interface
Q	volumetric flow rate
Q_A	volumetric flow rate in annular film
Q_0	volumetric flow rate in filled tube
r	radial co-ordinate
r^*	dimensionless radial co-ordinate
r_i	radial position of annular film interface
R	tube inner radius
Re	Reynolds number
S	shape function, Eqs. (23) and (24)
t	time
t_d^*	scaled time, Eq. (1)
u	mean velocity in draining annular film
U	mean velocity in filled capillary
U_s	velocity of slug front
V_{lens}	lens volume
$V_{YY'}$	lens volume (hemispherical meniscus), Fig. 4(b)
x_c	dimensionless radial position of annular film interface (annular film of thickness L_c)
x_i	dimensionless radial position of annular film interface, $x_i = r_i/R$
z	axial co-ordinate
z^*	dimensionless axial co-ordinate
z_b	lens distance below the tube exit plane at $r = 0$
z_b^*	dimensionless lens distance below the tube exit plane at $r = 0$, $z_b^* = z_b/R$

Greek

γ	surface tension
Γ	wetting rate
κ	curvature
μ	dynamic viscosity
θ	contact angle
ρ	density

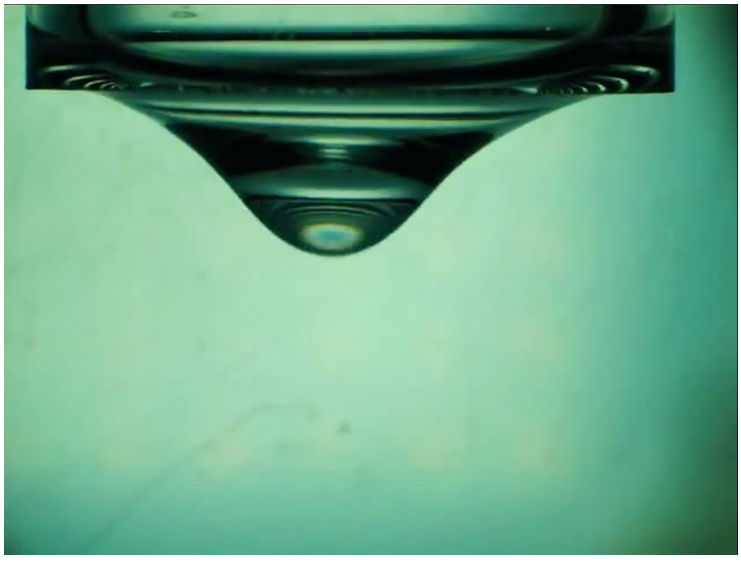

Video 1. Glycerol, $D = 21.6$ mm

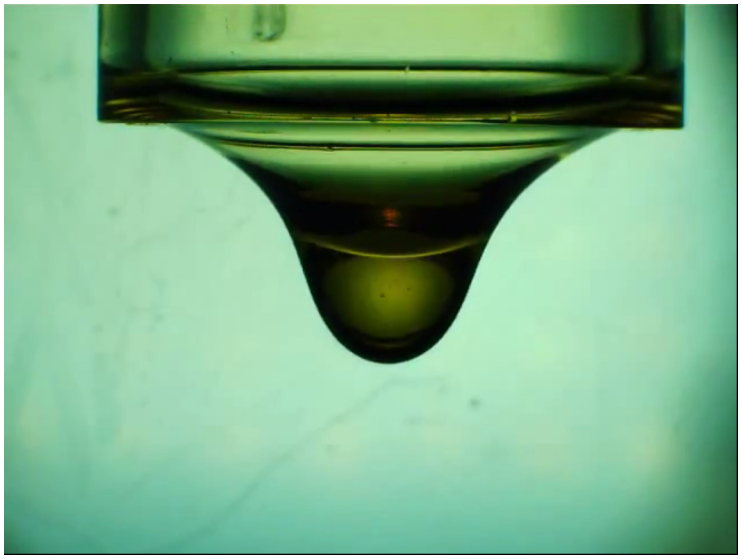

Video 2. Golden syrup, $D = 21.8$ mm

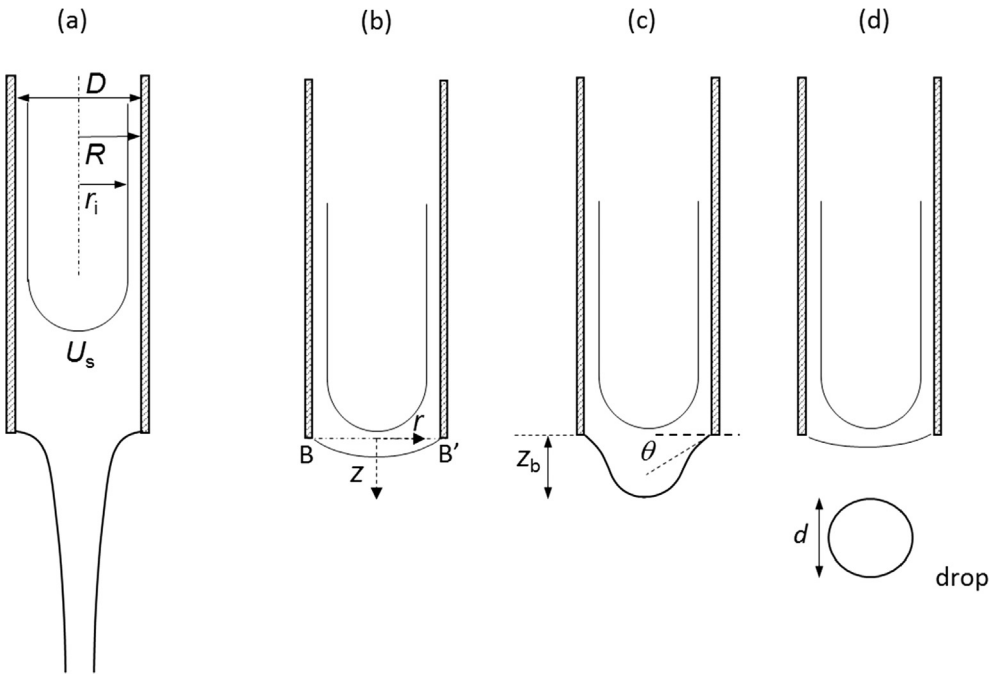

Fig. 1. Schematics of stages in lens formation and drop shedding, showing dimensions. (*a*) Initial steady drainage stage, with air slug descending at velocity U_s and liquid draining as a filament; (*b*) filament breaks yielding liquid lens at B-B′, the shape of which changes over time; (*c*) lens grows, extending distance z_b below the tube exit plane; (*d*) drop of diameter d is shed and remaining liquid reforms lens.

Images of the cycle are shown in Fig. 2, where time is presented in terms of scaled time, t_d^*, defined as

$$t_d^* \equiv \frac{\text{time elapsed since last drop}}{\text{period of time to shed current drop}} \quad (1)$$

such that $0 \le t_d^* \le 1$. The two series show that the evolution of drop shape differs between drops. This is because the flow rate in the draining annular film decreases with time, which affects the shape of the lens after drop formation. The evolution of lens shape for different cycles is presented quantitatively in Fig. 3. Here z_b is the depth of the lens at $r = 0$ below the plane B-B′ in Fig. 1 and R is the inner radius of the tube. As the flow rate decreases, the value of z_b^* ($= z_b/R$) at the start of the cycle approaches zero, *i.e.* the lens is initially almost flat. The lower interface is presumably pinned at inner edge of the tube, so the contact angle can be preserved while yielding a flat or even slightly concave interface: the configuration of the experiments reported here did not allow the end region to be imaged in great detail. Further examples for other liquids tested are available in the data archive.

Ali et al. [1] reported the transition to the lens formation and dropping regime for honey and two varieties of Marmite®, a non-Newtonian food spread. They did not analyse the formation of individual drops. This paper presents an investigation of the parameters determining drop behaviour, employing a number of different tube sizes and surfaces, for four Newtonian liquids. The data are reported in terms of a correlation obtained from dimensional analysis and compared with the predictions of a new simple model as well as a selection of models in the literature which have been developed for drops falling from narrow capillaries.

The authors are not aware of previous investigations of this phenomenon. The flow pattern exhibits axial symmetry so is likely to be amenable to analytical approaches as well as computational solutions.

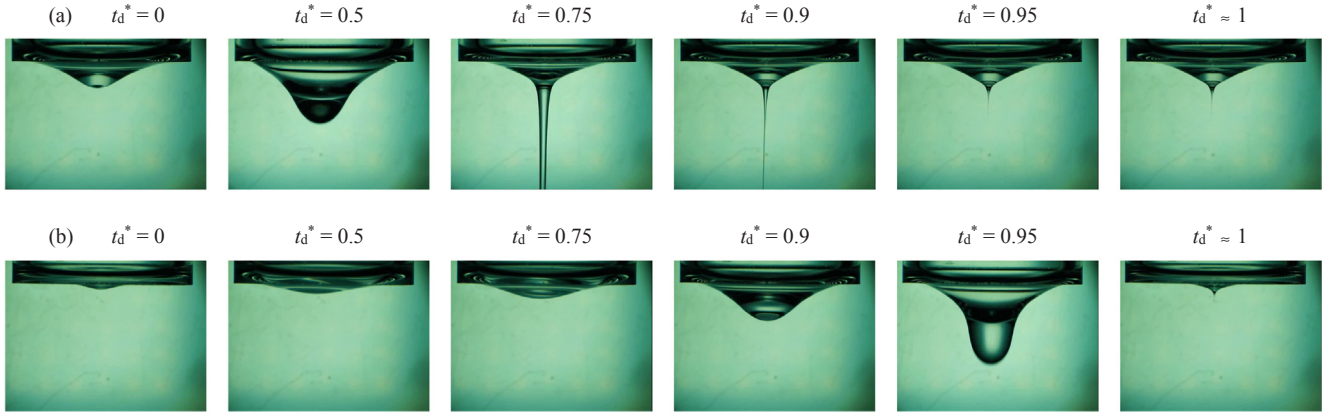

Fig. 2. Stages in the lens formation cycle and drop shedding extracted from video of glycerol, $D = 21.6$ mm glass tube at various scaled times, t_d^*, for (*a*) the second drop, lasting 0.28 s; and (*b*) the eighth drop, lasting 0.45 s.

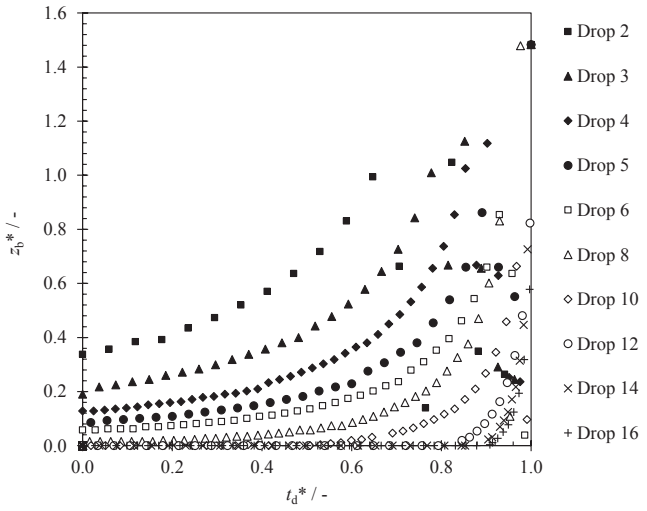

Fig. 3. Evolution of dimensionless lens size, $z_b^* = z_b/R$, against scaled cycle time, t_d^*, for glycerol, $D = 21.6$ mm glass tube (see Fig. 2).

It could be used as a test case for numerical codes which model interfacial dynamics. The data are available from an open data repository for other researchers to pursue such lines of investigation.

2. Modelling

2.1. Dimensional analysis

The mass of the drop, m, is measured during the experiments. m is reported in terms of the equivalent sphere diameter, d, calculated from $d \equiv \sqrt[3]{(6m/\rho\pi)}$ where ρ is the liquid density. The characteristic geometrical length scale of the system is the tube inner diameter, D, while the timescale is provided by gravitational acceleration, g. Fluid-related properties expected to affect drop formation are the liquid viscosity, μ, liquid-air surface tension, γ, and contact angle, θ. The mass flow rate of fluid entering the lens from the annular film, M, can be related to the mean velocity in the film, u, via the thickness of the film. These will be shown to be related to the other parameters. The problem statement is then

$$d = f(D,g,M,\mu,\rho,\gamma,\theta) \tag{2}$$

Falling films similar to those considered here are encountered in the evaporator literature, where the mass flow rate in a falling film is often expressed in terms of the wetting rate, $\Gamma \equiv M/\pi D$.

Selecting D, g and ρ as basis parameters yields 5 dimensionless groups, with a functional relationship to be determined

$$\frac{d}{D} = f_1(Fr,Ga,Bo,\theta) \tag{3}$$

Here the Froude number is defined $Fr \equiv M^2/\rho^2 D^5 g$, the Galilei number $Ga \equiv \rho^2 D^3 g/\mu^2$ and the Bond number $Bo \equiv \rho D^2 g/\gamma$.

Setting $Bo = 1$ yields the characteristic length scale in the fluid where surface tension forces balance gravity, known as the capillary length, $L_c \equiv (\gamma/\rho g)^{1/2}$, and the Bond number can be expressed as $Bo \equiv D^2/L_c^2$. The largest value of L_c for the liquids used in the experiments was 2.5 mm. The smallest tube radius was 3.8 mm, so surface tension effects are comparable with gravity and gravity will affect the shape of menisci.

The Galilei number is one form of dimensionless viscosity, which compares gravitational body force to the viscous forces in draining. The Morton number, defined $Mo \equiv g\mu^4/\rho\gamma^3$ (N.B. $Mo \equiv Bo^3/Ga^2$) is another group which could be used, which compares viscous forces to surface tension, and contains primarily fluid properties. Test fluids were selected which gave a wide range of Morton numbers, namely rapeseed oil, glycerol, honey and golden syrup (with $0.01 < Mo < 4 \times 10^5$). Their physical properties and the associated values of Mo, Bo and Ga for the experimental parameters are summarised in Table 1.

The nature of the experiments is such that M, and thus u, are set by the flow in the draining film and varies with time. The range of Fr values encountered are reported in Table 1. Inspection of the values in the Table shows that lens formation was associated with Bond numbers in the range of $10 \le Bo < 120$, a wide range of Ga ($0.05 < Ga < 5000$), and small Fr ($Fr < 10^{-4}$).

Inspection of the experimental data indicated that the effective sphere diameter, d, was strongly related to the capillary length, L_c, while the dependency on mass flow rate was captured more clearly when this was expressed in terms of the Reynolds number in the falling film, $Re \equiv 4M/\mu\pi D = (16FrGa/\pi^2)^{1/2}$.

Eq. (3) can be expressed as

$$\frac{d}{L_c} \equiv \frac{d}{D}Bo^{1/2} = f_2(Re,Ga,Mo,\theta) \tag{4}$$

The experimental data are interrogated to see whether the data follow a simple correlation of this form.

2.2. Capillary drop models

Several models exist for the mass of a drop, m, created by liquid leaving a filled capillary of radius R ($\equiv D/2$). These models are compared here with the experimental data for our case where liquid drains down the inner wall of a wide vertical tube, forming a lens that sheds

Table 1
Physical properties and dimensionless groups for test fluids.

Fluid	Rapeseed oil	Glycerol	Honey	Golden syrup
Density /kg m^{-3}	910 ± 10	1 260 ± 10	1 430 ± 10	1 410 ± 10
Viscosity /Pa s	0.08 ± 0.001	1.4 ± 0.01	10 ± 0.1	12 ± 0.1
Surface tension /mN m^{-1}	34 ± 5	64 ± 5	58 ± 5	80 ± 5
Contact angle				
Perspex (D = 7.6, 14.7, 21.8 mm)	22° ± 5	83° ± 5	81° ± 5	80° ± 5
Borosilicate glass (D = 8.7, 15.0, 21.6 mm)	27° ± 5	31° ± 5	72° ± 5	75° ± 5
Capillary length /mm	2.0	2.3	2.0	2.5
Mo	0.011	110	3.5×10^5	2.8×10^5
Bo				
D = 7.6 mm	15	11	14	10
D = 8.7 mm	20	15	18	13
D = 14.7 mm	57	42	52	37
D = 15.0 mm	59	43	54	39
D = 21.6 mm	123†	90	113	81
D = 21.8 mm	125†	92	115	82
Ga				
D = 7.6 mm	560	3.5	0.088	0.059
D = 8.7 mm	840	5.2	0.13	0.089
D = 14.7 mm	4 000	25	0.64	0.43
D = 15.0 mm	4 300	27	0.68	0.46
D = 21.6 mm	12 800†	80	2.0	1.36
D = 21.8 mm	13 200†	82	2.1	1.40
Fr				
D = 7.6 mm	$2.6–3\,400 \times 10^{-8}$	$3.4–470\,000 \times 10^{-10}$	$2.1–5\,300 \times 10^{-10}$	$1.1–390 \times 10^{-9}$
D = 15.0 mm	$1.0–130 \times 10^{-8}$	$4.6–640\,000 \times 10^{-11}$	$7.4–180\,000 \times 10^{-11}$	$9.6–5\,500 \times 10^{-10}$
D = 21.8 mm	–	$6.0–1\,700\,000 \times 10^{-12}$	$1.4–36\,000 \times 10^{-11}$	$1.3–700 \times 10^{-10}$
Re				
D = 7.6 mm	$4.8–170 \times 10^{-3}$	$4.4–1\,600 \times 10^{-5}$	$5.5–270 \times 10^{-6}$	$1.0–19 \times 10^{-5}$
D = 15.0 mm	$8.3–95 \times 10^{-3}$	$4.5–1\,700 \times 10^{-5}$	$9.0–1\,400 \times 10^{-6}$	$2.7–64 \times 10^{-5}$
D = 21.8 mm	–	$2.8–1\,500 \times 10^{-5}$	$6.9–1\,100 \times 10^{-6}$	$1.7–40 \times 10^{-5}$

† No lens formation occurred, only plug-like flow was observed.

drops periodically. When the flow rate is small, Wilson [13] stated that [11] formula,

$$m \equiv \rho\frac{\pi d^3}{6} = 3.8\frac{\gamma R}{g} \tag{5}$$

is a reasonable estimate. In practice this is adjusted by the Harkins and Brown correction factor [7]. This result can be expressed in dimensionless form, after some rearrangement, as

$$\frac{d}{L_c} = 1.54Bo^{1/6} \tag{6}$$

Wilson [13] considered the case of a drop formed when a pendant drop grows slowly, effectively under conditions of static equilibrium, until it reaches a critical value at which part breaks away to form a drop and the remainder recovers to form a smaller pendant drop, in a manner similar to Fig. 2(a). He obtained the result

$$m = 2.40\frac{\gamma R}{g} + \frac{\pi D^2}{4}\left(3\frac{\mu\rho}{g}U\right)^{1/2} \tag{7}$$

where U is the mean velocity in the capillary. This gives

$$\frac{d}{L_c} = \left[2.3Bo^{1/2} + 2.6Bo^{3/2}\left(\frac{Fr_c}{Ga}\right)^{1/4}\right]^{1/3} \tag{8}$$

The subscript on the Froude number indicates that the characteristic velocity is that associated with the flow in the capillary ($Fr_c \equiv U^2/gD$). This result captured the effect of flow rate observed experimentally for tests with golden syrup and a 3.5 mm diameter capillary, but underpredicted the drop mass systematically, by about 20%, and Wilson described several factors which could explain the discrepancy.

Zhang and Basaran [14] presented the following result for the mass of drops generated by a Newtonian liquid flowing slowly from a cylindrical capillary

$$m = 0.6\rho\left(\frac{\pi D\gamma}{\rho g} - \frac{4}{3}\frac{Q^2}{\pi R^2 g} + 7.14\left(\frac{Q^2R^2\gamma}{\rho g^2}\right)^{1/3}\right) \tag{9}$$

where Q is the volumetric flow rate. The second term on the RHS of Eq. (9) incorporates the effect of flow rate using reasoning similar to that of Wilson [13]. The third term arises from the consideration of flow into the drop during detachment, and was derived from fitting to experimental data. In dimensionless form, Eq. (9) can be expressed as

$$\frac{d}{L_c} = \left[3.6Bo^{1/2} - \frac{6}{5}Bo^{3/2}Fr_c + 4.4Bo^{7/6}Fr_c^{1/3}\right]^{1/3} \tag{10}$$

2.3. Simple quasi-static lens model

The experimental data sets are also compared with a simple model for the maximum mass of a drop which would be generated by a lens fed by a draining annular film. Fig. 4(a) shows the lens at the point of instability, where the mass of the drop and momentum flowing into the lens are balanced by surface tension acting at the tube rim and the annular film at X-X′. It is postulated that after shedding, the lens adopts the shape shown in Fig. 4(b), with a flat base and a meniscus with minimum thickness h resulting from capillary rise. The drop volume is calculated by difference. This simple model brings out some of the geometrical features involved.

The mass, and thus volume, of the lens at the point of instability is given by a force balance:

$$m_{lens}g + Mu = 2\pi r_i\gamma + \pi D\gamma\sin\theta \tag{11}$$

Writing $r_i/R = x_i$, following the terminology of Ali et al. [1], yields

$$m_{lens} + \frac{Mu}{g} = \frac{\pi D\gamma}{g}(x_i + \sin\theta) \tag{12}$$

Ali et al. [1] showed that the volumetric flow rate in the annular film,

Q_A, is given by[1]

$$Q_A = Q_0(1-4x_i^2 + 3x_i^4 - 4x_i^4 \ln x_i) \tag{13}$$

where Q_0 is the volumetric flow rate from a filled tube, *i.e.* before lens formation

$$Q_0 = \frac{\pi}{128}\frac{\rho g D^4}{\mu} \tag{14}$$

The mean velocity can then be calculated from

$$u = \frac{Q_A}{\frac{\pi}{4}D^2(1-x_i^2)}$$

$$= \frac{1}{32}\frac{\rho g D^2}{\mu}\frac{(1-4x_i^2 + 3x_i^4 - 4x_i^4 \ln x_i)}{(1-x_i^2)} \tag{15}$$

and the mass flow rate of fluid entering the lens from the annular film can be expressed as

$$M \equiv \rho Q_A = \frac{\pi}{128}\frac{\rho^2 g D^4}{\mu}(1-4x_i^2 + 3x_i^4 - 4x_i^4 \ln x_i) \tag{16}$$

Hence

$$Mu = 0.00077\frac{\rho^3 g^2 D^6}{\mu^2}\frac{(1-4x_i^2 + 3x_i^4 - 4x_i^4 \ln x_i)^2}{(1-x_i^2)} \tag{17}$$

Substituting (17) into (12) gives the volume of the lens at the critical point as

$$V_{lens} = \frac{\pi D\gamma}{\rho g}(x_i + \sin\theta) - 0.00077\frac{\rho^2 g D^6}{\mu^2}\frac{(1-4x_i^2 + 3x_i^4 - 4x_i^4 \ln x_i)^2}{(1-x_i^2)} \tag{18}$$

The volume of liquid in the lens below Y-Y′ in Fig. 4(b), $V_{YY'}$, can be calculated readily if the meniscus is hemispherical. For wide capillaries, the meniscus will not be hemispherical: its shape is determined by *Bo* and must be determined numerically, as reported by Concus [6]. For the data presented in the Results section, $V_{YY'}$ was calculated numerically following the method of Concus [6], and the arithmetic mean value was used for each data set. Hence

$$V_{lens} = \frac{\pi D\gamma}{\rho g}(x_i + \sin\theta) - 0.00077\frac{\rho^2 g D^6}{\mu^2}\frac{(1-4x_i^2 + 3x_i^4 - 4x_i^4 \ln x_i)^2}{(1-x_i^2)} - V_{YY'} \tag{19}$$

Expressing the volume as a drop size gives

$$\left(\frac{d}{D}\right)^3 = \frac{6}{Bo}(x_i + \sin\theta) - 0.0015Ga\frac{(1-4x_i^2 + 3x_i^4 - 4x_i^4 \ln x_i)^2}{(1-x_i^2)} - \frac{6}{\pi D^3}V_{YY'} \tag{20}$$

Or, in terms of the capillary length

$$\frac{d}{L_c} = Bo^{1/2}\left[\frac{6}{Bo}(x_i + \sin\theta) - 0.0015Ga\frac{(1-4x_i^2 + 3x_i^4 - 4x_i^4 \ln x_i)^2}{(1-x_i^2)} - \frac{6}{\pi D^3}V_{YY'}\right]^{1/3} \tag{21}$$

For the purposes of illustration, the result for the hemispherical case is

$$h = \frac{2\gamma}{\rho g r_i} \tag{22}$$

Hence

$$V_{YY'} = \frac{\pi}{4}D^2\left(r_i + \frac{2\gamma}{\rho g r_i}\right) - \frac{2\pi}{3}r_i^3$$

$$= \frac{\pi D^3}{6}\left(\frac{3}{4}x_i + \frac{6}{Bo}x_i^{-1} - \frac{1}{2}x_i^3\right)$$

$$= \frac{\pi D^3}{6}S\left(x_i, Bo\right) \tag{23}$$

where S is a function linked to the shape of the meniscus, which is in turn determined by x_i and *Bo*. Substituting (23) into (21) gives

$$\frac{d}{L_c} = Bo^{1/2}\left[\frac{6}{Bo}(x_i + \sin\theta) - 0.0015Ga\frac{(1-4x_i^2 + 3x_i^4 - 4x_i^4 \ln x_i)^2}{(1-x_i^2)} - \underbrace{\frac{3}{4}x_i - \frac{6}{Bo}x_i^{-1} + \frac{x_i^3}{2}}_{S(x_i,Bo)}\right]^{1/3} \tag{24}$$

The shape function S is expected to exhibit a more complex dependency on *Bo* and x_i.

It should be noted that Eqs. (20) and (21) incorporate a dependency on *M* via x_i: the flow rate in the annular film determines x_i, as shown in Eq. (16). In dimensionless form, Eq. (16) can be expressed as

$$\frac{Fr}{Ga} = \left[\frac{\pi}{128}(1-4x_i^2 + 3x_i^4 - 4x_i^4 \ln x_i)\right]^2 \tag{25}$$

Combining Eqs. (20) and (25) (to eliminate x_i) results in an expression of a form consistent with Eq. (3).

3. Methods and materials

3.1. Tubes and drainage test

The polymethylmethacrylate (Perspex™) and borosilicate glass tubes used by Ali et al. [1] were employed in this work. The dimensions of the tubes are given in Table 1. Short tubes were used as the emphasis was on the drop formation regime. A bung was inserted in the bottom end of the tube and the liquid added slowly to avoid entrapping air bubbles. The mass of the tube and bung before and after filling was recorded. After filling, each tube was left to stand vertical, overnight, in order to promote disengagement of any air bubbles present.

Before a test the tube was located vertically above a receiving dish mounted on a datalogging mass balance and the alignment checked with an electronic spirit level. A USB microscope was mounted level with the tube exit and focused on the exit. The tube was backlit for image contrast. Video capture at 26 fps and mass recording were started before the bung was removed and continued until drops stopped forming. The response time of the balance was measured and found to be short compared to the time between drops. After a test the tube was rinsed out with tap water, cleaned thoroughly with detergent solution, rinsed in hot water then dried.

Video capture was not performed for all experiments. The microscope was focussed on the base of the tube: the field of view did not allow the shape of extending filaments and shed drops to be imaged.

3.2. Test fluids

Glycerol was obtained from Sigma Aldrich. The golden syrup used was a lower viscosity ('squeezy') own-brand product purchased from a local supermarket. The honey was a clear variety and, like the rapeseed oil, was obtained from a supermarket. Fluid densities were measured at 20 °C using a 25 ml volumetric flask with an error of ± 0.04 ml and a Precisia XB3200C weighing scale with error of ± 0.01 g.

Fluid viscosities were measured at 20 °C on a Malvern Kinexus rotational rheometer fitted with rough parallel plates using a gap height of 1 mm and apparent shear rates ranging from 0.01 to 100 s^{-1}. The

[1] There is an error in Ali et al.'s Eq. (10), in the last term on the RHS.

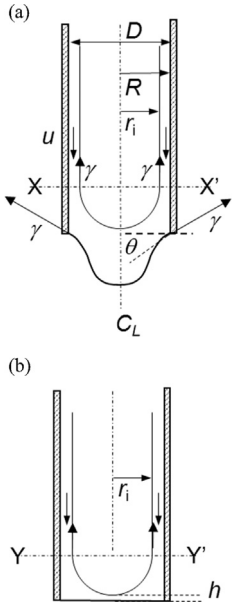

Fig. 4. Schematic of simple lens model. (*a*) Force balance giving lens mass at point of instability; (*b*) geometrical construction giving volume of stationary lens. The meniscus is drawn as circular for illustration.

glycerol and rapeseed oil were Newtonian, while the golden syrup and honey exhibited a small degree of shear thinning across this range. For the shear rates employed in the experiments, at $\leq 1.9\,s^{-1}$ for the golden syrup and $\leq 4.4\,s^{-1}$ for the honey, the liquids were effectively Newtonian.

The surface tension for glycerol was taken from the literature [12]. The surface tension of the other fluids was extracted from filament thinning tests on a Cambridge Trimaster HB4 extensional rheometer. The diameter of the filament, F, was compared to the result for a Newtonian liquid,

$$\frac{F(t)}{F(t=0)} = 1 - \frac{0.4254\gamma t}{3\mu F(t=0)} \tag{26}$$

and γ calculated using the measured viscosity. The values obtained were similar to those in the literature, with the exception of golden syrup: the measured value of $85 \pm 5\,mN\,m^{-1}$ was larger than the $80\,mN\,m^{-1}$ reported by Llewellin et al. [9] for a syrup with density $1440\,kg\,m^{-3}$, so the literature value was used. The symbol size for the golden syrup data reflects this uncertainty.

Contact angles were measured with a DataPhysics goniometer using the sessile drop technique. Flat Perspex and borosilicate glass slides were used. Small drops of the test fluids (drop diameter $< L_c$) were placed on the slides and allowed to settle for 10–20 min, checking whether the shape changed at two minute intervals. The contact angle was then extracted using the inbuilt camera and software. In all the experiments, the test fluids were observed to wet the tube materials ($\theta < 90°$). The measured contact angles were consistent with the observations, except for honey on Perspex, where the measured contact angle was non-wetting. This discrepancy may be due to differences in Perspex composition and surface texture. A literature value for the contact angle of honey on Perspex of $\theta = 81°$ [1] was therefore used. The results indicate that the substrate nature did not have a large effect.

3.3. Mass flow rates

The mass flow rate, M, for each drop was estimated by fitting a quadratic equation to the total mass of drops collected,

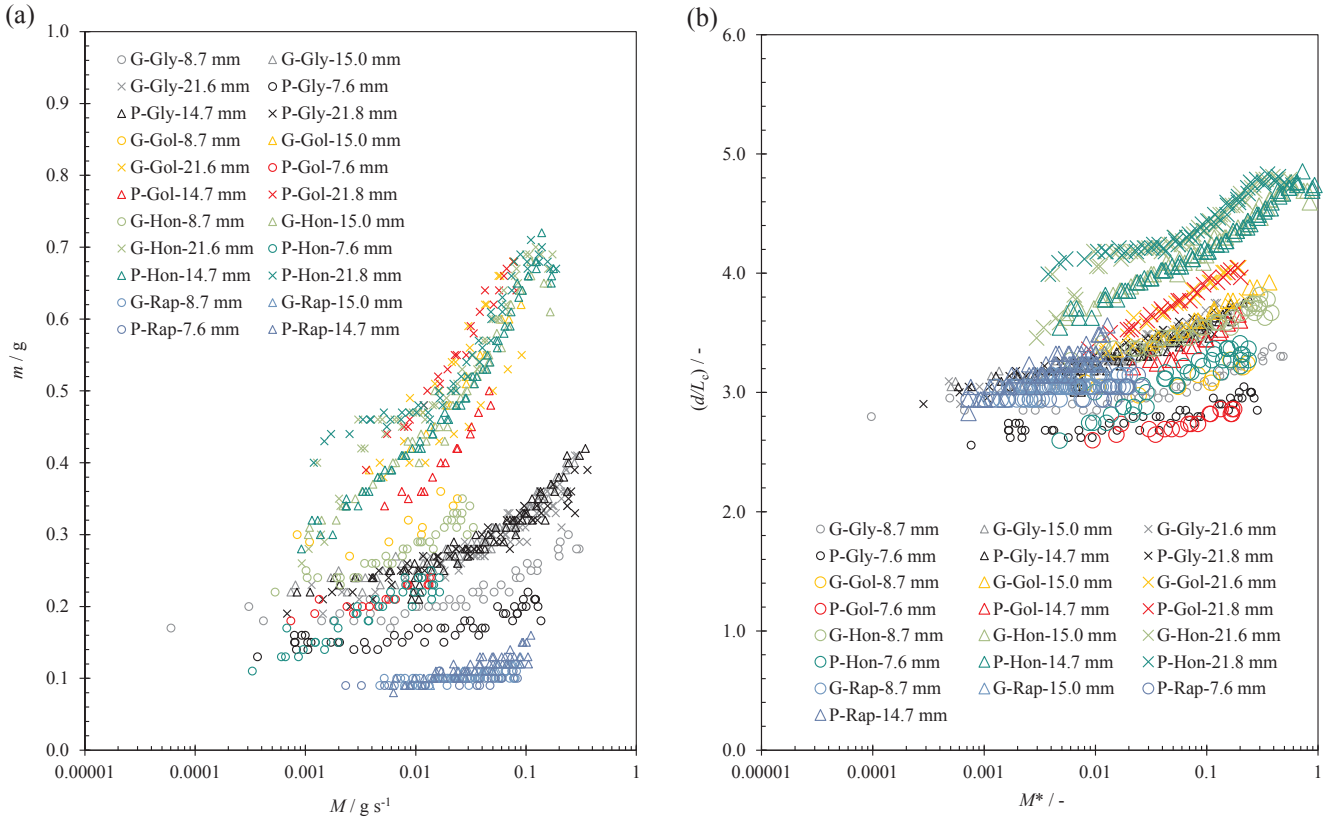

Fig. 5. Effect of test fluid and tube diameter on equivalent droplet size. (*a*) Evolution of drop mass, m, with mass flow rate in the annular film, M, (*b*) Evolution of drop equivalent sphere diameter, d, scaled by the capillary length, L_c, with dimensionless mass flow rate in the annular film M^* ($=M/M_c$). Labels indicate tube material (G, glass; P, Perspex) – liquid – D. Symbol size is related to the measurement uncertainty.

$$m_{total} = a_1 t^2 + a_2 t + a_3 \quad (27)$$

and differentiating this to give the instantaneous flow rate, *viz.*

$$M = 2a_1 t + a_2 \quad (28)$$

3.4. Video analysis

Frame by frame analysis was performed using the OpenCV library for Python. For each frame, the location of the tube base and edges was marked and the Canny Edge [5] detection method was used to generate an edge map. The centreline of the tube was identified and the cylindrical co-ordinates of the lower lens interface identified. The interface was symmetrical in virtually all cases. The volume of the lens protruding below the tube end could then be calculated.

A quintic spline was fitted to the interface data in order to evaluate the curvature of the interface, κ, from [10]:

$$\kappa = \frac{\frac{dr}{dz}}{z\left(1+\left[\frac{dr}{dz}\right]^2\right)^{3/2}} + \frac{\frac{d^2r}{dz^2}}{\left(1+\left[\frac{dr}{dz}\right]^2\right)^{3/2}} \quad (29)$$

The local hydrostatic pressure on the liquid side of the interface, $P_{L,int}$, at coordinates (r, z) was then determined from

$$P_{L,int} = P_{atm} + \gamma\kappa \quad (30)$$

and the pressure in the liquid at the tube outlet, P_b (*i.e.* where $z = 0$) calculated using

$$P_b(z=0) = P_{L,int} - \rho g z \quad (31)$$

This allowed the distribution of the pressure in the liquid across the base of the tube to be evaluated. An example is given in Fig. 9.

4. Results and discussion

4.1. Overall behaviour

Table 1 shows that lens formation and dripping was observed in all the tubes for glycerol, honey and golden syrup, but not in the 21.6 and 21.8 mm tube for rapeseed oil, which had both the lowest viscosity and smallest surface tension. In the tubes of the largest diameter, plug-like flow was observed for rapeseed oil experiments: no lens formation occurred. After rapid emptying of the bulk of the oil, dripping occurred from the tube rims. In the widest tubes, gravity-driven flow dominated over surface tension and viscous effects, resulting in the absence of lens formation.

Fig. 5(a) presents the data from all tests, which are available via the data repository. The drop mass increases with the mass flow rate for each fluid, as predicted by the Wilson model, albeit with different trends for each fluid and tube size. In each test, the drop size gets smaller with time as the thickness of, and thus flow rate in, the draining film decreases. In many cases the drop size appears to approach a limiting value, but detailed inspection of the data sets indicated that this was not a universal feature.

Inspection of these data in terms of d/D tended to separate sets on the basis of D as the drop masses (and hence diameter) are quite similar. Fig. 5(b) shows that when plotted as d/L_c, the capillary length scale emerges as a characteristic length scale, with the data lying in the range $2.5 < d/L_c < 5$. This is noticeably similar to the values calculated using Eq. (6), which gave $2.2 < d/L_c < 3.4$ for the range of Bo involved in these experiments. This model does not predict any dependency on flow into the drop, which Wilson reported as tending to increase the mass of the drop and hence its diameter.

The mass flow rate is reported in Fig. 5(b) as the fraction of that expected for a falling film with thickness L_c, where $M^* = M/M_c$, and M_c is calculated by setting x_i in Eq. (16) as $x_i = 1 - L_c/R$. The scaled mass flow rates all lie below 1, indicating that this value could be used as a threshold for when lens formation and dropping start.

Very low flow rates were not studied as these entailed long experimental runs. The period between drops in Fig. 5 ranged from 0.8 s to 4 min.

The figure shows that the nature of the liquid and mass flow rate affect drop size significantly. By comparison, the nature of the wall has little effect. The slight difference in the diameters of the glass and Perspex tubes means that the effect of contact angle could not be determined precisely.

4.2. Dimensional analysis

The models incorporating mass flow rate dependency (Eqs. (8), (10) and (21)) all take the form of a series of terms. The data were plotted in the forms suggested by Eqs. (3) and (4), using different expressions for the series based on the models, but a consistently superior formulation was not obtained.

The capillary drop models in the literature take the form of a static term involving Bo and a flow term. The static term was selected such that this contribution was always smaller than d/L_c. A non-biased approach was applied and non-linear regression used to identify coefficients. This yielded the correlation

$$\frac{d}{L_c} = 1.35Bo^{1/6} + 1.3(\sin\theta)^{-0.09}\, Re^{0.18}\, Mo^{0.12} \quad (32)$$

Fig. 6 shows the fit to the data ($R^2 = 0.82$, mean % difference = 5.6%). There is considerable scatter evident and some data sets deviate systematically from the above relationship, indicating that Eq. (32) did not capture all aspects of the physics. The values of R^2 and the mean percentage difference for individual data sets are summarised in Table 2.

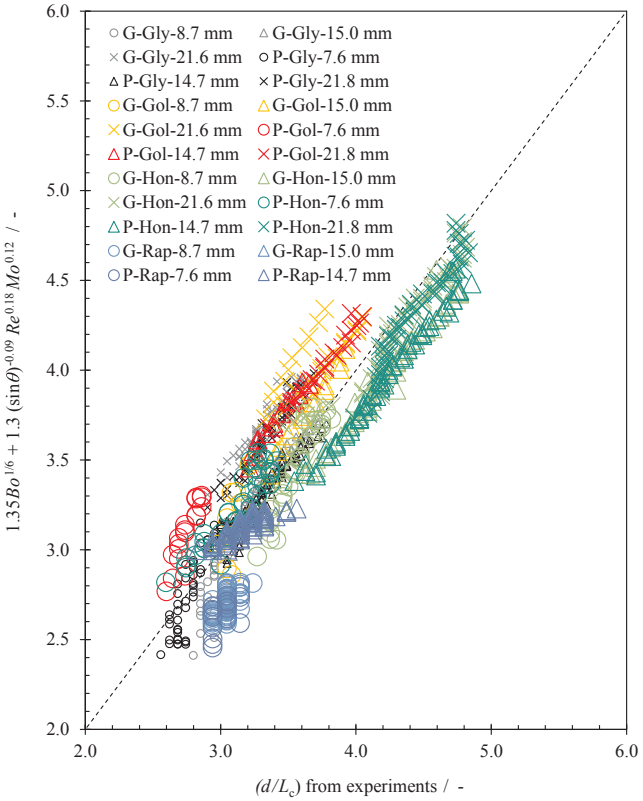

Fig. 6. Fit of correlation (Eq. (32)) to the experimental results for various test fluids and tube diameters. The dashed line is the line of equality. Labels indicate tube material (G, glass; P, Perspex) – liquid – D. Symbol size is related to the measurement uncertainty.

Table 2
Values of regression coefficient R^2 and the mean percentage difference between the experimental data and Eq. (32).

	Rapeseed oil		Glycerol		Honey		Golden syrup	
	R^2	% difference	R^2	% difference	R^2	% difference	R^2	% difference
D = 7.6 mm	0.25	12	0.79	4.1	0.86	4.2	0.81	12
D = 8.7 mm	0.39	11	0.86	3.4	0.90	3.3	0.59	5.6
D = 14.7 mm	0.77	3.0	0.90	1.7	0.98	6.4	0.96	8.9
D = 15.0 mm	0.90	1.4	0.93	1.5	0.97	6.1	0.99	3.7
D = 21.6 mm	–	–	0.90	11	0.90	2.8	0.65	9.6
D = 21.8 mm	–	–	0.93	8.7	0.93	3.3	0.97	7.0

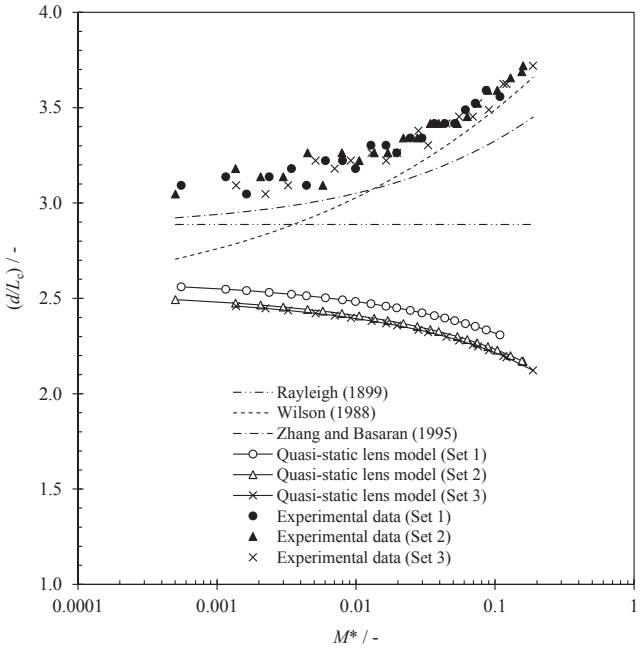

Fig. 7. Evolution of drop equivalent sphere diameter, d, scaled by the capillary length, L_c, with dimensionless mass flow rate in the annular film M^* ($=M/M_c$). Comparison between the experimental data for glycerol, D = 15.0 mm glass tube, with the models of Rayleigh (Eq. (6)), Wilson (Eq. (8)), Zhang and Basaran (Eq. (10)), and the simple quasi-static lens model (Eq. (24)). Supplementary Fig. 1 shows similar comparison for golden syrup, D = 15.0 mm glass tube.

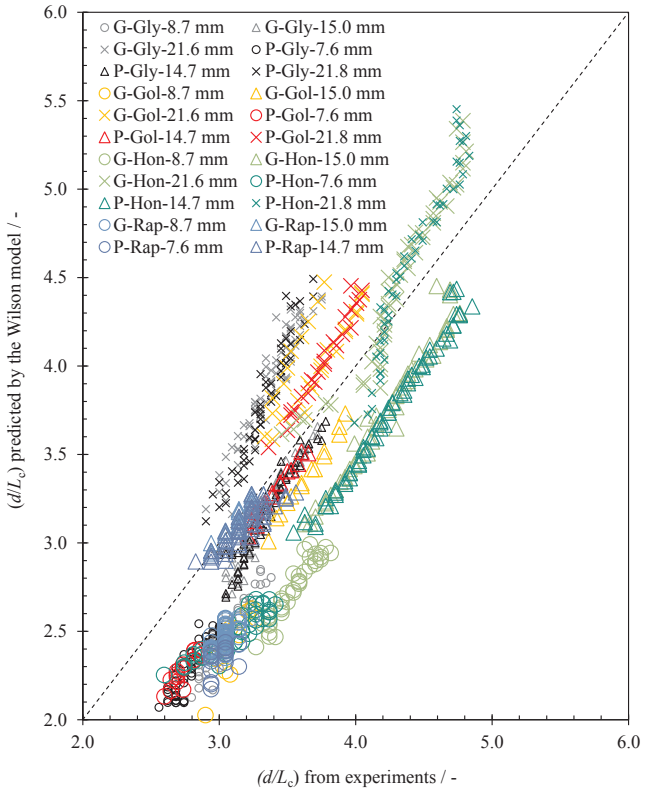

Fig. 8. Agreement between the Wilson model (Eq. (8)) and experimental results. The dashed line is the line of equality. Labels indicate tube material (G, glass; P, Perspex) – liquid – D. Symbol size is related to the measurement uncertainty.

4.3. Comparison with existing models

Each data set was compared with the predictions for d/L_c obtained using the existing models for drop formation from capillaries and the quasi-static lens model, given by Eqs. (6), (8), (10) and (21). In the predictions, the mean velocity in the draining annular film, u, estimated from M using Eqs. (15) and (16), was used as the characteristic velocity in calculating Fr_c. The Rayleigh model result is independent of flow rate, so both Fig. 5 and Eq. (32) indicate that it will give poor agreement with the experimental results. Fig. 7 shows one example where the data are compared with the models. A second is provided as Supplementary Fig. 1. The Rayleigh model provides an estimate of the limit at negligible flow. The quasi-static lens model predicts a decrease in d/L_c for increasing M^*, indicating that the geometric concept is not correct. The data exhibit a similar trend to the Wilson model. Other data sets (different fluid, D and surface) are provided in the data archive.

Fig. 8 compares all the experimental d/L_c data with the prediction of the Wilson model for each case. By comparison, the mean deviation from the empirical correlation (Fig. 6) was 5.6% whereas for the Wilson model (Fig. 8) this was 12%. The model underestimates d/L_c for the smaller diameter tubes, reflecting the pattern reported by Wilson for (smaller) capillaries: as D increases, the model tends to over-predict the drop size. One of the reasons for this is the different dependencies in flow rates: Wilson considered a filled tube feeding the drop, where the flow rate is proportional to D^4, whereas the flow rate in the annular film is proportional to $D\times$(film thickness)^3, see Ali et al. [1]. Moreover, at the point of drop formation there are two free surfaces in the lens dropping case, that external to the drop and that of the meniscus above the lens. The surface tension contribution from the meniscus differentiates this process from other cases of drop formation.

4.4. Mechanistic insight

The shape of the meniscus and the lens clearly plays a role in determining the drop size, allied with the momentum entering the lens. Further analysis is required to capture the dynamics of the lens. Some insight is provided by image analysis of the lens and the initial stages of drop formation.

Fig. 9 shows an example of the shape of the meniscus and the pressure in the liquid at the tube outlet, P_b (*i.e.* where z = 0), calculated using Eq. (31) for one case at one point in time. P_b was found to be

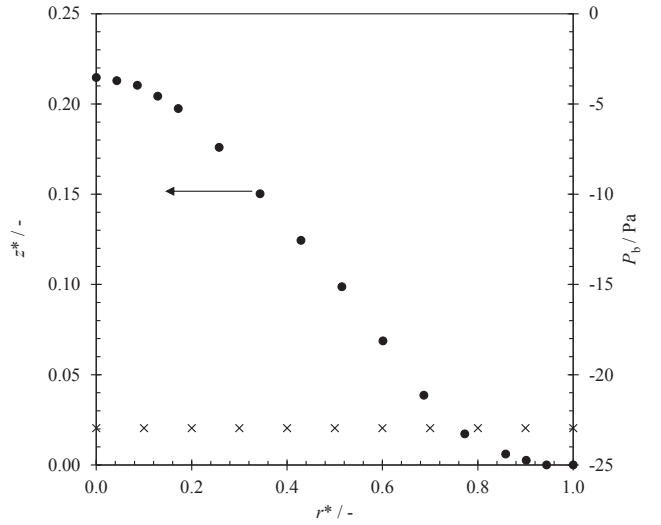

Fig. 9. Example of dimensionless lens shape, z^* ($=z/R$), and the gauge pressure in the liquid at the tube outlet, P_b, against tube radius, r^* ($=r/R$) for glycerol, $D = 21.6$ mm glass tube, eighth drop, $t_d^* = 0.5$.

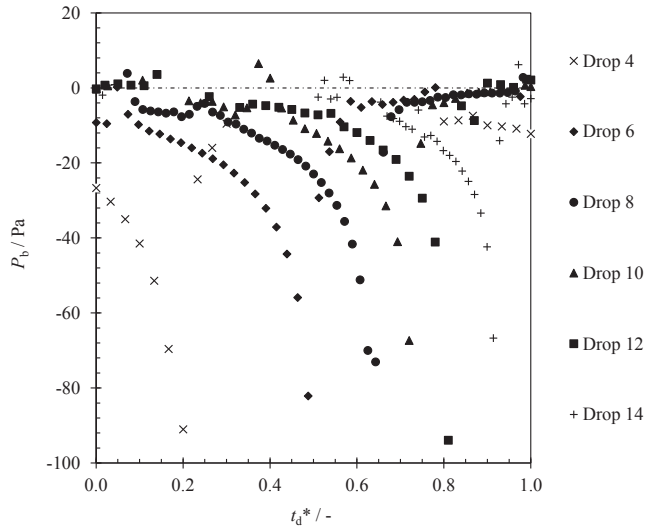

Fig. 10. Evolution of gauge pressure in the liquid at the tube outlet, P_b, for different drops in the series for glycerol, $D = 21.6$ mm glass tube. Supplementary Fig. 2 shows data for glycerol, $D = 15.0$ mm glass tube.

uniform along the base of the tube at a given time, independent of the shape of the meniscus. Similar results were observed for other instants and other cases. This indicates that the shape of the lens is consistent with fluid statics up to the point where the lens becomes unstable and extends into a wide filament.

The evolution of P_b over time for different drops in the series is shown in Fig. 10 for glycerol in a 21.6 mm glass tube. Similar trends were observed in the other cases studied. For a given drop, P_b decreases over time, corresponding to the lens sagging further beneath the tube rim as it collects more liquid until it becomes unstable. The lowest value of P_b captured is approximately -80 Pa for $D = 21.6$ mm (see Fig. 10). The lowest value for $D = 15$ mm lay around -60 Pa (see Supplementary Fig. 2). The rapid decrease in P_b corresponds to the transition to the formation of the elongated drop (see Fig. 2(b), $t_d^* = 0.95$). This occurs at increasing values of t_d^* for successive drops.

The minimum in P_b accompanying drop shedding is followed by a period where P_b is close to atmospheric, when the falling drop is attached by a thin filament and the lens has otherwise returned to the initial state. Other data sets (different fluid, D, and surface) are provided in the data archive.

The criterion for the limit of lens stability was not identified here but the pressure provides some insight into the transition. The lens is initially almost flat and draining liquid accumulates in the meniscus within the tube. As the lens grows, it starts to sag and this gives rise to a negative pressure in the liquid at the plane B-B′(Fig. 1(b)). This causes liquid to flow across the plane from the meniscus and collect in the lens: the lens becomes nipple shaped (Fig. 1(c)) and P_b then decreases more quickly as liquid is added, accelerating drainage of the meniscus. When the rate of drainage across B-B′ is larger than the rate of flow into the meniscus from the falling film, the level of the meniscus drops and it eventually crosses the plane B-B′. The shape of the lens below B-B′ is no longer constrained solely by contact with the tube rim and the shape can change noticeably, giving rise to a neck similar to that described by Wilson in his tests. In several of the videos, the transition to necking was accompanied by the meniscus level passing below B-B′ but the camera was not configured to capture this feature reliably: further work is required on the apparatus to make this reliable.

5. Conclusions

The shedding of individual drops of viscous Newtonian liquids from the lens formed at the end of an open draining tube was investigated. This cyclic process followed three stages; growth of a sagging lens which eventually became unstable; shedding of an extended drop; followed by thinning of a narrow filament. The length of each stage depended on the rate of drainage into the drop, and the drop mass was found to increase modestly with flow rate.

Analysis of the data indicated that the capillary length, L_c, was a more suitable characteristic length scale than the tube diameter. The equivalent drop diameter, d, data for two tube materials, three diameters and four liquids lay in the range $2.5 < d/L_c < 5$. The data were fitted to an empirical correlation for d/L_c, with a mean deviation of 5.6%. The data were compared with models in the literature for droplet formation from narrower, filled capillaries and a new quasi-static lens model. Wilson's model gave closest agreement (with a mean deviation of 12%) as well as reflecting the general trend more reliably.

The results indicate that the dynamics of the lens requires further investigation, building on the Wilson model. Image analysis of the lens confirmed that its shape was consistent with fluid statics up to the point of extension. The shedding of a drop is associated with the lens shape changing as the meniscus falls below the end of the tube. The raw data are provided for other researchers to investigate this behaviour.

Acknowledgements

An EPSRC studentship for GLC is gratefully acknowledged, as is a Newnham & Principal's Studentship for MWLC from Newnham College, Cambridge.

Appendix A. Supplementary material

A range of video files and the data used to create the plots in this manuscript are available from the University of Cambridge data repository at (doi: http://dx.doi.org/10.17863/CAM.22310) under the Open Data initiative. Supplementary data associated with this article can be found, in the online version, at http://dx.doi.org/10.1016/j.expthermflusci.2018.04.015.

References

[1] A. Ali, A. Underwood, Y.-R. Lee, D.I. Wilson, Self-drainage of viscous liquids in vertical and inclined pipes, Food Bioprod. Process. 99 (2016) 38–50.
[2] N.J. Balmforth, N. Dubash, A.C. Slim, Extensional dynamics of viscoplastic filaments: I. Long-wave approximation and the Rayleigh instability, J. Non-Newtonian Fluid Mech. 165 (2010) 1139–1146.
[3] N.J. Balmforth, N. Dubash, A.C. Slim, Extensional dynamics of viscoplastic

filaments: II. Drips and bridges, J. Non-Newtonian Fluid Mech. 165 (2010) 1147–1160.
[4] J.D. Berry, M.J. Neeson, R.R. Dagastine, D.Y.C. Chan, R.F. Tabor, Measurement of surface and interfacial tension using pendant drop tensiometry, J. Coll. Interf. Sci. 454 (2015) 226–237.
[5] J. Canny, A computational approach to edge detection, IEEE Trans. Pattern Anal. 8 (6) (1986) 679–698.
[6] P. Concus, Static menisci in a vertical right circular cylinder, J. Fluid Mech. 34 (1968) 481–495.
[7] W.D. Harkins, F.E. Brown, The determination of surface tension (free surface energy), and the weight of falling drops: the surface tension of water and benzene by the capillary height method, J. Am. Chem. Soc. 41 (1919) 499–524.
[8] B.-B. Lee, P. Ravindra, E.-S. Chan, A critical review: surface and interfacial tension measurement by the drop weight method, Chem. Eng. Commun. 195 (2008) 889–924.
[9] E.W. Llewellin, H.M. Mader, S.D.R. Wilson, The rheology of a bubbly liquid, Proc. Royal Soc. London Series A – Math. Phys. Eng. Sci. 458 (2002) 987–1016.
[10] A. Lopez de Ramos, R.A. Redner, R.L. Cerro, Surface tension from pendant drop curvature, Langmuir 9 (12) (1993) 3691–3694.
[11] Lord Rayleigh, XXXVI investigations in capillarity – the size of drops – the liberation of gas from supersaturated solutions - colliding jets – the tension of contaminated water surfaces, Phil. Mag. Series 5, 48(293) (1899), 321–337.
[12] E.W. Washburn, International Critical Tables of Numerical Data, Physics, Chemistry and Technology (1st Electronic Edition), Knovel, (2003), accessed at https://app.knovel.com/hotlink/toc/id:kpICTNDPC4/international-critical/international-critical.
[13] S.D.R. Wilson, The slow dripping of a viscous fluid, J. Fluid Mech. 190 (1988) 561–570.
[14] X. Zhang, O. Basaran, An experimental study of dynamics of drop formation, Phys. Fluids 7 (6) (1995) 1184–1203.